Hot Deformation and Dynamic Recrystallization of Ti-6Al-7Nb Biomedical Alloy in Single-Phase β Region

F. Pilehva, A. Zarei-Hanzaki, S.M. Fatemi-Varzaneh, and A.R. Khalesian

The aim of this investigation is to evaluate the hot deformation behavior and critical conditions for onset of dynamic recrystallization in Ti-6Al-7Nb biomedical alloy. The effects of temperature and strain rate on the hot deformation behavior of Ti-6Al-7Nb alloy were studied by employing hot compression tests. The experiments were conducted at temperatures of 1050, 1100, and 1150 °C under strain rates of 0.0025, 0.025, and 0.25 s^{-1} up to a true strain of 0.65. The evolution of compressive flow stress during deformation of the experimental alloy in the single-phase β region was investigated. The obtained microstructures showed the occurrence of partial dynamic recrystallization along the prior grain boundaries, which was discussed relying on the continuous recrystallization process. Using the strain-hardening rate curves ($d\sigma/d\varepsilon$ versus σ), two characteristic parameters including the critical strain for DRX initiation (ε_c) and the strain for peak stress (ε_p) were identified. The normalized critical stress and strain for initiation of DRX were, respectively, found to be 0.9 and 0.67. True stress-true strain curves have been used to construct proper constitutive equations for the experimental alloy. The obtained activation energy for hot deformation was discussed considering the dominant restoration processes. Moreover, the flow stress was modeled for different strain levels, where good agreement with the experimental alloy was found.

1. Introduction

Titanium-based alloys have been known to be promising materials for implant applications due to the combination of outstanding characteristics such as high strength, low density (high specific strength), high immunity to corrosion, complete inertness to body environment, enhanced biocompatibility, low modulus, and high capacity to join with bone and other tissues (Ref 1). Annealed Ti-6Al-4V alloy has been the most common titanium alloy used for biomedical device manufacture. However, continued concern with respect to the biological response of vanadium-containing materials (Ref 2) has led to the development of many titanium-based alloys of Nb, Zr, Ta, Sn, Pd with various percentages (Ref 3, 4). Ti-6Al-7Nb alloy is one of the most attractive titanium biomaterial alloys developed based on the well-known Ti-6Al-4V by replacing vanadium by niobium in its chemical composition (Ref 5).

The best strategy employed to invoke desired microstructure and mechanical properties in titanium alloys includes optimized cycles of hot working and heat treatment. Primary hot working to produce a uniformly wrought microstructure is usually conducted at temperature range of single-phase beta. Therefore, careful process control and profound knowledge of the influence of processing condition on the flow behavior and

final microstructure are of great importance for the manufacturing of titanium alloy products of good performance.

Over the last decades, finite element (FE) simulation has been successfully used as a tool to analyze and optimize the thermomechanical processes (Ref 6, 7). Constitutive equations are used as inputs to the FE code for simulating the material's response under specified loading conditions (Ref 8). Therefore, the accuracy of the FE simulation depends, to a large extent, on the accuracy of the deformation behavior of the material which is being represented by the constitutive equations (Ref 9).

Basically, constitutive equation is a mathematical representation of the relationship between the flow behavior of the material and the process parameters like strain (ε), strain rate ($\dot{\varepsilon}$), and temperature (T). Most of these constitutive relationships are either phenomenological or empirical in nature (Ref 10). In the phenomenological approach, proposed by Sellars and McTegart (Ref 11), the flow stress is expressed by the sine-hyperbolic law in an Arrhenius type of equation, which has been extensively used to predict high-temperature flow behavior (Ref 12-14). In case of flow behavior modeling of titanium alloys, Shafaat et al. (Ref 15). and Cai et al. (Ref 16). have modeled the flow behavior of Ti-6Al-4 V alloy in two-phase and single-phase regions.

Also, some researches may be found in the literature dealing with the effect of thermomechanical processing on the flow behavior and microstructure evolution of Ti-6Al-4V (Ref 17-19). However, quite rare studies have been found in the literature on the hot deformation characteristics of Ti-6Al-7Nb alloy and related effect of thermomechanical parameters. Cui et al. (Ref 20). investigated the hot deformation behavior of Ti-6Al-7Nb in two-phase α + β region. The results indicated that dynamic recrystallization (DRX) occurred during compressive deformation at two-phase region of 750-950 °C. Nevertheless, no systematic investigation has been conducted to characterize deformation behavior of the biomaterial in single-phase β region. It is worth recalling that the primary thermomechanical process-

F. Pilehva, A. Zarei-Hanzaki, and **A.R. Khalesian**, School of Metallurgy and Materials Engineering, College of Engineering, University of Tehran, Tehran, Iran; and **S.M. Fatemi-Varzaneh**, Shahid Rajaee Teacher Training University, Tehran, Iran. Contact e-mail: zareih@ut.ac.ir.

ing is usually performed at high temperatures, where β phase is thermodynamically stabilized.

The present work was aimed to assess the effect of temperature and strain rate on the flow behavior of Ti-6Al-7Nb through modeling the flow stress in single-phase β region, where the critical condition for onset DRX has been also determined. Moreover, the model was modified compensating the effect of strain.

2. Materials and Procedure

The experimental material used in this study was received as rods in mill-annealed condition with 10 mm in diameter. The chemical composition of the alloy was 5.9Al, 6.75Nb, 0.03Fe, 0.16O, 0.002N, 0.02C, 0.002H (wt.%), balanced Ti. As it is shown in Fig. 1, the microstructure of the as-received bar was bimodal, i.e., the equiaxed alpha in a matrix of transformed beta. The related beta-transus temperature is about 1020 °C (Ref 21). To evaluate the deformation behavior, compression testing method was performed at temperatures of 1050-1150 °C and strain rates of 0.0025, 0.025, and 0.25 s^{-1}. Cylindrical compression specimens of 15 mm height and 10 mm diameter were machined from the as-received rods. The hot compression tests were conducted using a Gotech AI-7000 universal testing machine coupled with a programmable resistance furnace. Prior to any hot compression test, the specimens were soaked at the deformation temperature for 7 min to equilibrate the temperature throughout the specimens. The specimens were then hot compressed up to a true strain of 0.65 followed by immediate quenching in water to preserve the deformed microstructures. A thin layer of mica was placed between the face of the specimen and the anvils in order to maintain the uniform deformation and avoid sticking problems during quenching. The deformed specimens were sectioned parallel to the compression axis and prepared for metallographic examinations using standard procedures. Metallographic samples after grinding, polishing, and etching were characterized using optical microscope. Kroll's reagent consisting of 1-2 ml HNO_3, 3-6 ml HF, and H_2O (in 100 ml reagent) was used to etch the specimens.
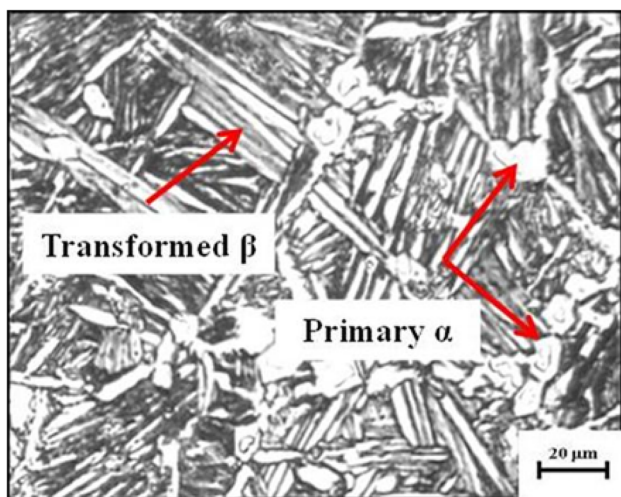

Fig. 1 The initial microstructure of Ti-6Al-7Nb experimental alloy

3. Results and Discussion

3.1 Flow Behavior

Typical true stress-true strain curves obtained during hot compression tests of Ti-6Al-7Nb in the single-phase β region are presented in Fig. 2. Most of the flow curves exhibit an initial increase in the stress with the increasing strain until a peak stress value is attained beyond which an apparently steady-state stress is observed. The latter denotes the operation of dynamic restoration processes counteracting material work hardening. These curves also reveal that the flow stress decreases with increasing deformation temperature, and increases with increasing strain rate at a given temperature.

To specify the operative restoration mechanism, the method developed by Poliak and Jonas (Ref 22) was employed for the present results. According to them, the initiation of dynamic recrystallization is governed by both energetic and kinetic critical conditions. The former requires that the energy stored during a given deformation schedule attain its maximum, while the latter requires the dissipative processes associated with deformation to decelerate to a critical level. Plotting $(d\theta/d\sigma)$ versus σ may provide useful information of the kinetic critical condition, where θ is the strain-hardening rate $(d\sigma/d\varepsilon)$. The latter introduces a minimum value of $-(d\theta/d\sigma)$ versus σ, when the critical state for DRX is attained and to the appearance of an inflection point in the θ-σ curve. Thus, the $-(d\theta/d\sigma)$ versus σ and θ-σ curves at different deformation conditions were constructed and are depicted in Fig. 3. As is seen, all the curves except the one that corresponds to 1050 °C/strain rate of 0.25 s^{-1} have definite inflection point which is an indication of DRX. On the other hand, all the curves have minimum point in their $-(d\theta/d\sigma)$ versus σ curves that may confirm the occurrence of DRX in all deformation conditions. This is further confirmed using microstructural investigation where the development of new grains (partial RX) was traced after straining at different conditions (Fig. 4).

The shape of stress-strain curves indicates some features which help to identify the restoration mechanisms involved during hot deformation. The occurrence of DRX is traditionally identified from the presence of stress peaks in flow curves (Ref 23). However, not all materials undergone DRX display well-defined peaks when tested under hot-working conditions (Ref 24). In this investigation, none of the curves showed distinct peak stress, but broad peaks or stress plateau. This kind of flow stress behavior in the beta phase field shows a resemblance to that of materials undergoing dynamic recovery (DRV) in which the rate of hardening by generation of dislocations is balanced by the rate of softening due to dislocation annihilation (Ref 25). The serrated grain boundaries, arrowed in Fig. 4, may also propose DRV as the dominant restoration mechanism of beta phase. Similar results were reported for titanium alloy in beta phase field (Ref 26, 27). Thus assuming the prevalence of dynamic recovery, it may be inferred that the nucleation of new grains formed along the initial grain boundaries (see Fig. 4) is the result of extended recovery invoked at the vicinity of boundaries i.e., continuous DRX. Consistently, previous research on the deformation behavior of titanium alloys in beta phase filed explained that the small recrystallized grains at the vicinity of the deformed grain boundaries are developed through continuous recrystallization process (Ref 28).

To better analyze the evolution of DRX process, the simple method developed by Najafizadeh and Jonas (Ref 29) was used
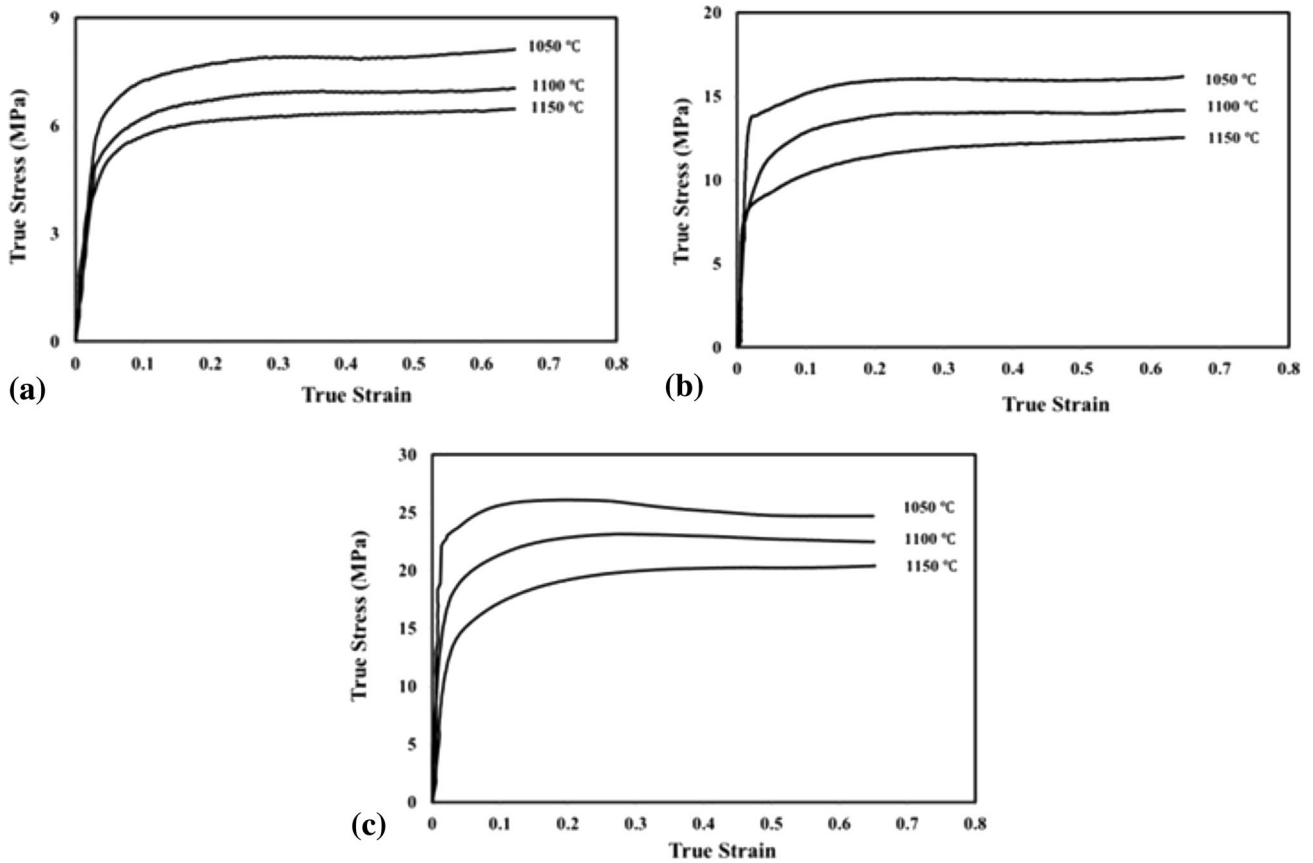
Fig. 2 The true stress-strain curves under strain rate of (a) 0.0025 s^{-1}, (b) 0.025 s^{-1}, and (c) 0.25 s^{-1} obtained by the isothermal compression test

for determining the critical stress for initiation of DRX. The inflection point is detected by fitting a third-order polynomial to the θ-σ curves up to the peak point as follows:

$$\theta = A\sigma^3 + B\sigma^2 + C\sigma + D$$

where A, B, C, and D are constants for a given set of deformation conditions. The second derivative of this equation with respect to σ can be expressed as

$$\frac{d^2\theta}{d\sigma^2} = 6A\sigma + 2B$$

at critical stress for initiation of DRX, the second derivative becomes zero and thereby

$$\sigma_c = -B/3A$$

Accordingly, this method was used to determine the value of critical stress at different deformation conditions. Using the flow curves, the values of critical strain were determined. The results are shown in Fig. 5. According to Fig. 5, the normalized critical stress and strain can be presented as

$$\sigma_c/\sigma_p = 0.9$$

$$\varepsilon_c/\varepsilon_p = 0.67$$

The critical stress for onset DRX increases by increasing strain rate and decreasing deformation temperature. This could

be related to the enhanced role of thermally activated recovery process in higher deformation temperatures and lower strain rates. The obtained values corresponding to the normalized critical stresses and strains are in good agreement with the reported ones for other titanium alloys (Ref 30).

3.2 Constitutive Equations

The hyperbolic-sine Arrhenius type constitutive equation is used to describe the correlation between flow stress (s), strain rate ($\dot{\varepsilon}$), and temperature (T). The temperature compensated strain rate, Zener-Hollomon parameter (Z) can be expressed as a hyperbolic-sine function of stress. These are given below.

$$Z = \dot{\varepsilon}\exp\left(\frac{Q}{RT}\right) \tag{Eq 1}$$

$$\dot{\varepsilon} = A[\sinh(\alpha\sigma)]^n \exp\left(\frac{-Q}{RT}\right) \tag{Eq 2}$$

where R is the universal gas constant (8.314 J/mol/K), T is the absolute temperature in K, Q is the activation energy (kJ/mol), and n is a material constant. Equation 2 is applicable in the entire stress range, since the hyperbolic-sine function reduces to a power-law at low stresses and an exponential at higher stresses. Accordingly, the power-law behavior at low stresses (valid for $\alpha\sigma < 0.8$) and the exponential stress dependence at high stresses (applicable for $\alpha\sigma > 1.2$) are given as
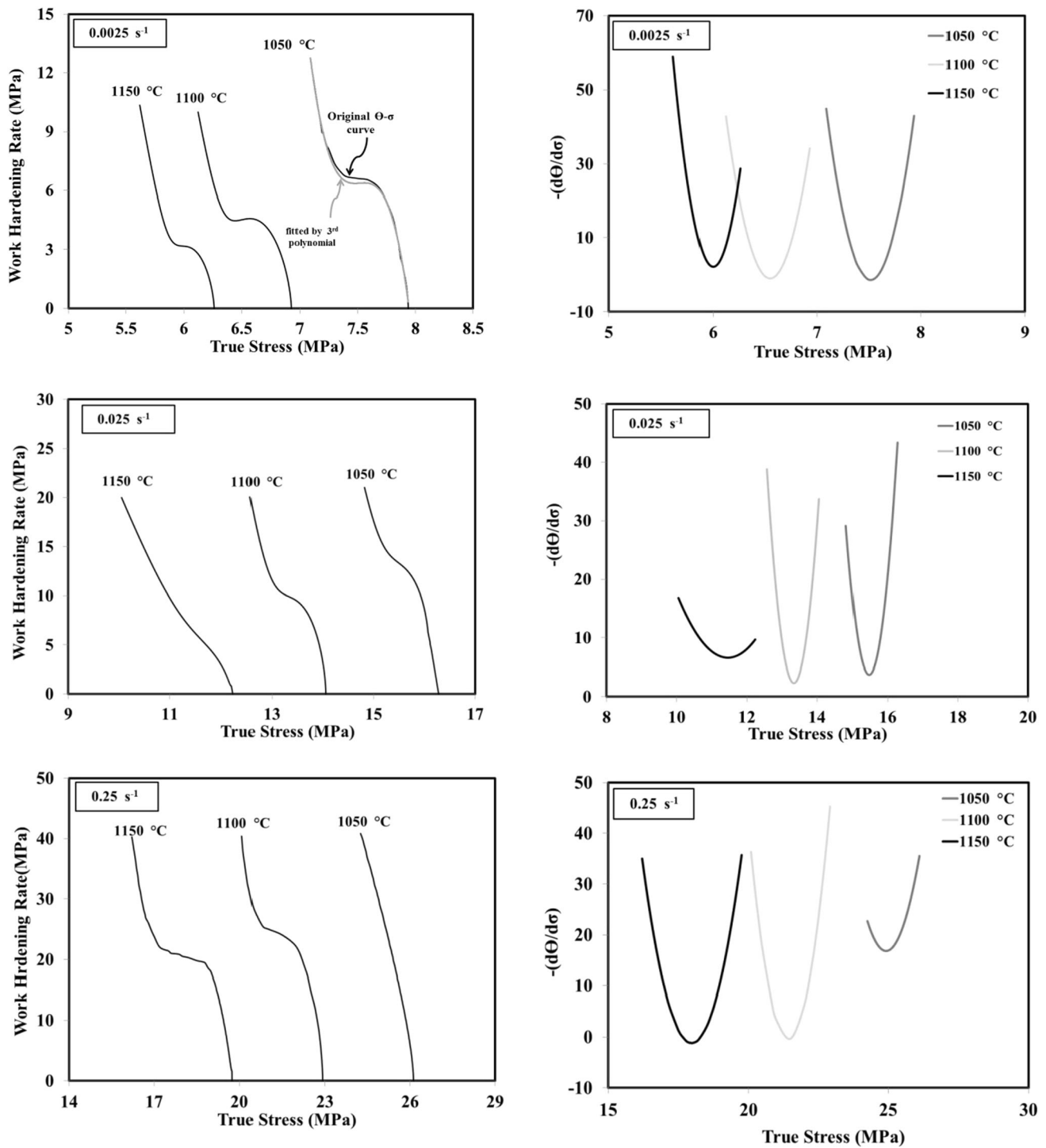
Fig. 3 Flow stress dependence of the strain-hardening rate and $-(d\theta/d\sigma)$ at different temperatures and strain rates

$$\dot{\varepsilon} = A'\sigma^{n_1} \exp\left(\frac{-Q}{RT}\right) \qquad \text{(Eq 3)}$$

$$\dot{\varepsilon} = A'' \exp(\beta\sigma) \exp\left(\frac{-Q}{RT}\right) \qquad \text{(Eq 4)}$$

$A, A', A'', \beta, n_1, \alpha$ are the material constants ($\alpha = \beta/n_1$). As is well understood, the effect of strain on the stress level would

not be considered in Eq 2. To precisely predict the flow stress behavior, the influence of strain should be incorporated. This has been done in the present work by considering the related material constants as functions of imposed strain.

3.2.1 Evaluation of Material Constants. True strain of 0.2 was selected as an example to introduce the solution procedures of the material constants. Taking the logarithm of both sides of Eq 3 and 4, respectively, gives
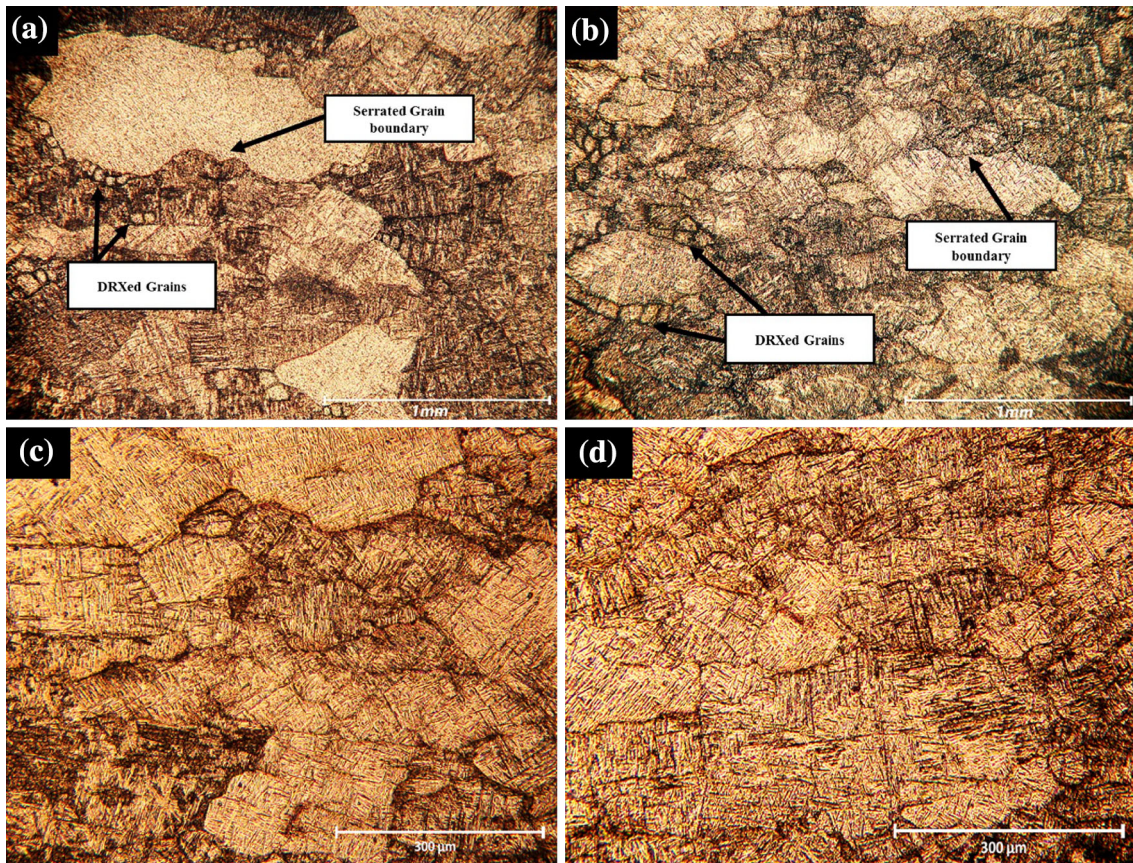
Fig. 4 Microstructures of deformed specimens at (a) 1050 °C (b) 1150 °C under strain rate of 0.0025 s^{-1} (c) 0.0025 s^{-1} (d) 0. 25 s^{-1} at 1100 °C
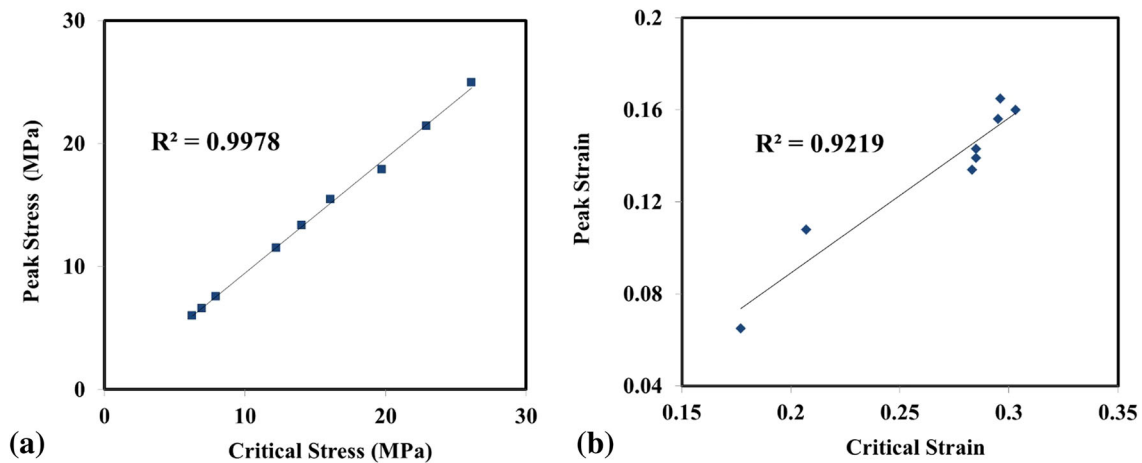
Fig. 5 (a) Peak stress vs. critical stress and (b) peak strain vs. peak strain

$$\ln(\sigma) = \frac{1}{n_1}\ln(\dot{\varepsilon}) - \frac{1}{n_1}\ln(A') \qquad \text{(Eq 5)}$$

$$\sigma = \frac{1}{\beta}\ln(\dot{\varepsilon}) - \frac{1}{\beta}\ln(A'') \qquad \text{(Eq 6)}$$

Then, substituting the values of the flow stress and corresponding strain rate under the strain of 0.2 into the logarithm Eq 5 and 6 gives the relationship between the flow stress and strain rate. As it can be seen in Fig. 6, flow stresses obtained from the compression tests can be approximated by a group of parallel and straight lines in the hot deformation conditions. The value of n_1 and β can be obtained from the slope of the lines in $\ln\sigma - \ln\dot{\varepsilon}$ and $\sigma - \ln\dot{\varepsilon}$ plots, respectively. Because the slope of the lines is approximately the same; the value of n_1 and β can be obtained for different deformation temperatures by linear fitting method, and a mean value of n_1 and β can be computed as 4.937 and 0.156 MPa^{-1}, respectively. Then, $\alpha = \beta/n_1 = 0.031$ MPa^{-1}.

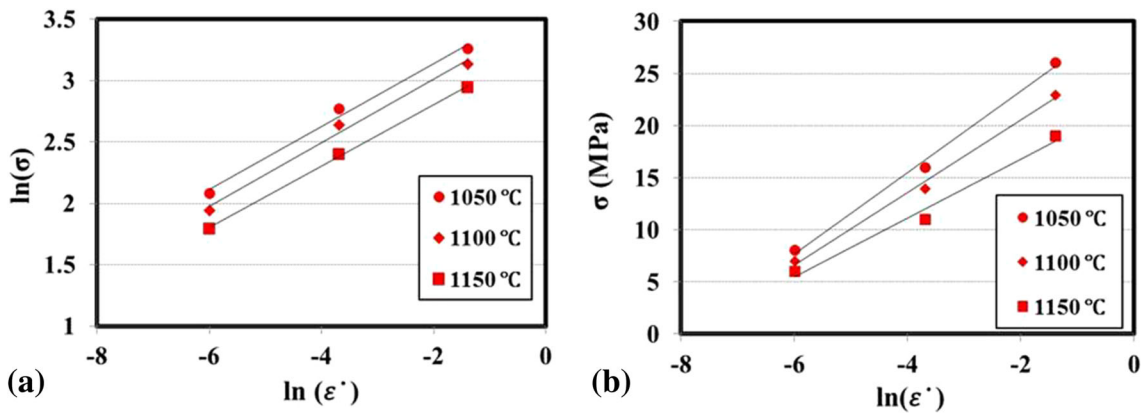**Fig. 6** The relationship between (a) ln(σ) and ln $\dot{\varepsilon}$, and (b) σ and ln $\dot{\varepsilon}$
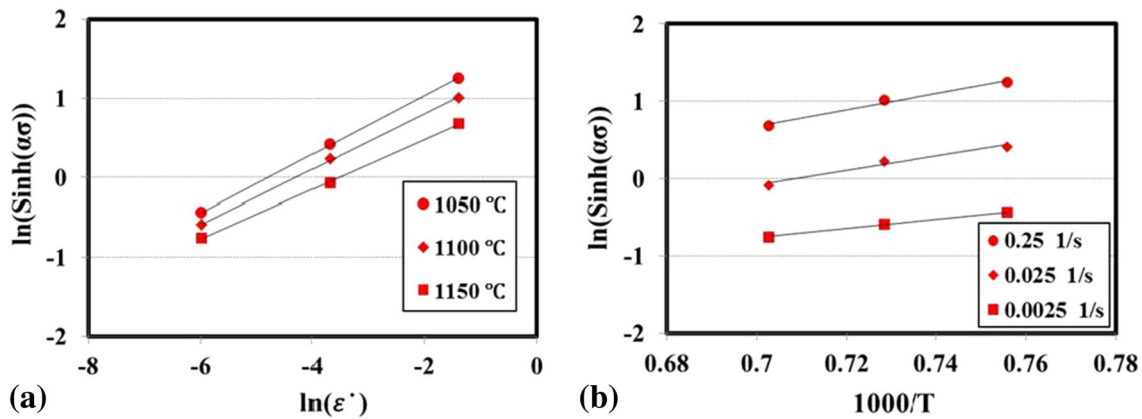

Fig. 7 The relationship between (a) ln[sinh ($\alpha\sigma$)] and lnε, and (b) ln[sinh ($\alpha\sigma$)] and 1000/T

Table 1 The obtained Q values for selected titanium alloys

Alloy	Type	Q parameter (kJ/mol)
Ti600 (Ti-6Al-2.8Sn-4Zr-0.5Mo-0.4Si-0.1Y) (Ref 31)	Near α	Q = 239
TA15(Ti-6Al-2Zr-1Mo-1V) (Ref 33)	Near α	Q = 219
Ti-15-3 (Ti-15V-3Cr-3 Sn-3 Al) (Ref 34)	Metastable β	Q = 199.9-245.6
Ti-6Al-4V (Ref 35)	$\alpha + \beta$	Q = 210-290
Ti-13V-11Cr-3Al (Ref 36)	β	Q = 213
Present study	$\alpha + \beta$	Q = 161-242

The value of α is in good agreement with the previous investigation (Ref 31, 32).

Taking the logarithms of both sides of the above Equation results in

$$\ln[\sinh(\alpha\sigma)] = \frac{\ln\dot{\varepsilon}}{n} + \frac{Q}{(nRT)} - \frac{\ln A}{n} \qquad (Eq\ 7)$$

The slope of ln [sinh ($\alpha\sigma$)] versus ln $\dot{\varepsilon}$ yields 1/n (Fig. 7a) and for a particular strain rate, differentiating Eq 8 results in

$$Q = \mathrm{R}n\left[\frac{\partial \ln[\sinh(\alpha\sigma)]}{\partial \frac{1}{T}}\right]_{\dot{\varepsilon}} \qquad (Eq\ 8)$$

Therefore, the values of activation energy (Q) are determined from the slopes of ln [sinh ($\alpha\sigma$)] versus 1/T

(Fig. 7b) through averaging the values under different strain rates. The ln$A$ is also easily found from the interception of ln [sinh($\alpha\sigma$)] versus ln $\dot{\varepsilon}$. The activation energy is obtained to be in the range of 161-242 kJ/mol for different strain values in temperature range of 1050-1150 °C (i.e., in the single-phase β region). The apparent activation energy is well above than that reported for self-diffusion in β phase (153 kJ/mol). Table 1 represents the reported activation energies for different titanium alloys during hot deformation in the β phase region. It is generally accepted that when dynamic recovery is the dominant mechanism during hot deformation, the activation energy for deformation is equal or close to that of self-diffusion (Ref 34). The higher activation energies, compared to the self-diffusion value, obtained in this study can be explained through the fact that solute and interstitial
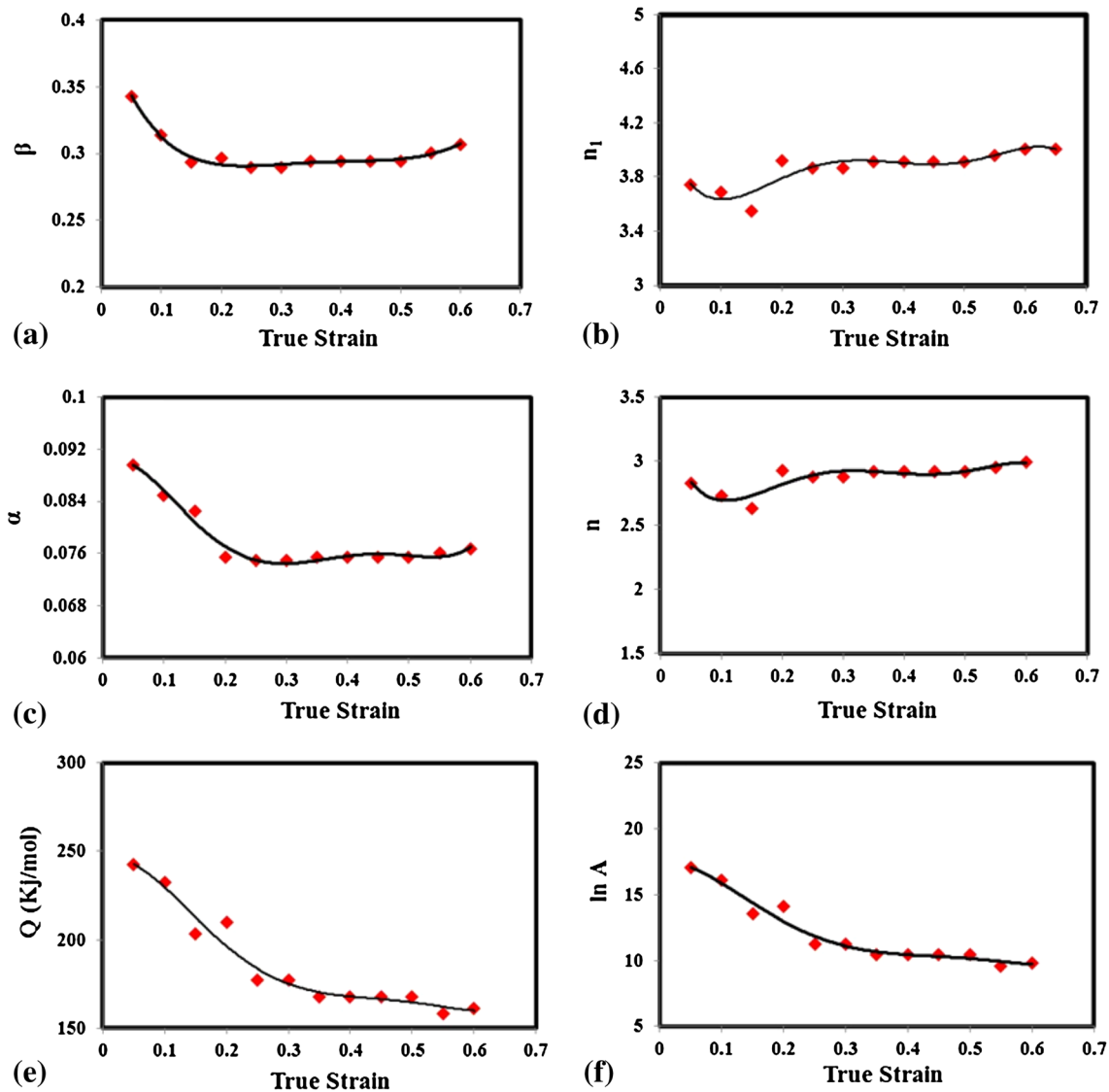
Fig. 8 The variation of biomedical Ti-6Al-7Nb constants (a) β, (b) n_1, (c) α, (d) n, (e) Q, and (f) $\ln A$ with true strain

atoms influence the diffusivity of the alloys. These interstitial atoms form the Cottrell atmosphere and limit the dislocation mobility (Ref 37). Moreover, the solute atoms act as barriers for dislocation movement, increasing the deformation resistance and thereby activation energy. The higher activation energy than energy of self-diffusion commonly attributed to occurrence of dynamic recrystallization which also supported by microstructural observations (Ref 38).

3.2.2 Compensation of Strain. The influence of strain on the constitutive equation is incorporated by assuming that the activation energy (Q) and material constants (i.e., n_1, β, α, n, and $\ln A$) are polynomial function of strains. In the present work, the values of the material constants have been evaluated relying on experimental data at various strains (in the range of 0.05–0.6) for the intervals of 0.05. The obtained results are presented in Fig. 8. These values are then employed to fit the polynomial function. A fifth-order polynomial, as shown in Eq 9, is found to represent the influence of strain on the material constants with a very valid correlation and generalization.

$$\beta = -4.7983x^5 + 14.453x^4 - 14.575x^3 + 6.6293x^2 - 1.381x + 0.3975$$

$$n' = -312.96x^5 + 586.17x^4 - 401.87x^3 + 121.39x^2 - 14.562x + 4.2224$$

$$\alpha = 8.2128x^5 - 13.451x^4 + 7.7579x^3 - 1.7358x^2 + 0.0687x + 0.0896$$

$$n = -349.31x^5 + 634.76x^4 - 425x^3 + 126.75x^2 - 15.481x + 3.3425$$

$$Q = 14494x^5 - 26899x^4 + 17835x^3 - 4681x^2 + 180.83x + 243.31$$

$$\ln A = 1121.3x^5 - 2107x^4 + 1407x^3 - 366.34x^2 + 10.429x + 17.286$$

$$(\text{Eq } 9)$$

Once the material constants are evaluated, the flow stress (σ) can be written as a function of Zener-Hollomon parameter. So,
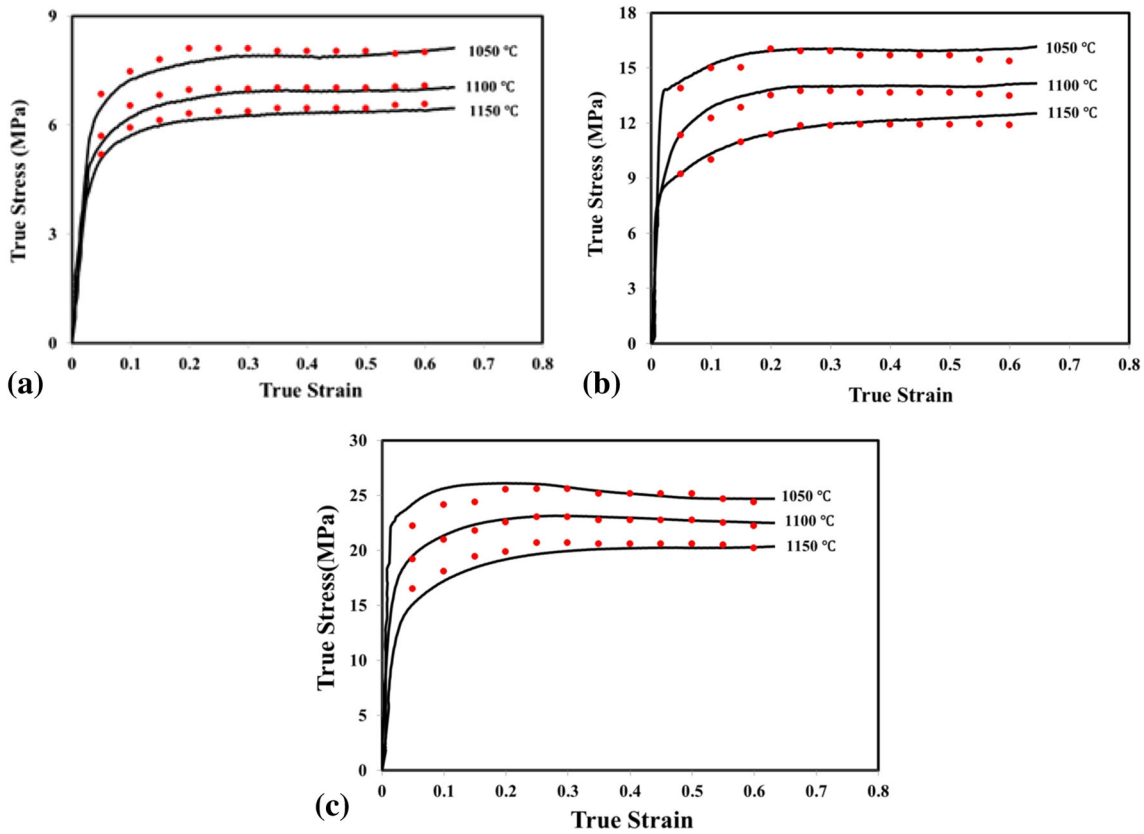
Fig. 9 The comparisons between predicted (dots) and measured flow stress curves (solid lines) of the Ti-6Al-7Nb biomedical alloy under the strain rates of (a) 0.0025 s^{-1}; (b) 0.025 s^{-1} and (c) 0.25 s^{-1}

the proposed constitutive model can be summarized as following (considering Eq 1 and 2):

$$\sigma = \frac{1}{\alpha}\ln\left\{ \left(\frac{Z}{A}\right)^{1/n} + \left[\left(\frac{Z}{A}\right)^{2/n} + 1\right]^{1/2}\right\} \quad \text{(Eq 10)}$$

3.2.3 Verification of the Model. In order to verify the developed constitutive equation of Ti-6Al-7Nb at elevated temperatures, a comparison between the experimental and predicted flow stress by the developed constitutive equation (considering the compensation of strain) is depicted in Fig. 9.

As shown in this figure, there is a good agreement between the experimental and predicted values. The accuracy of the constitutive equation is also further verified via employing standard statistical parameters such as correlation coefficient R and average absolute relative error (AARE). They are expressed as

$$R = \frac{\sum_{i=1}^{N}(E_i - \bar{E})(P_i - \bar{P})}{\sqrt{\sum_{i=1}^{N}(E_i - \bar{E})^2 \sum_{i=1}^{N}(P_i - \bar{P})^2}} \quad \text{(Eq 11)}$$

$$\text{AARE}(\%) = \frac{1}{N}\sum_{i=1}^{N}\left|\frac{E_i - P_i}{E_i}\right| \times 100 \quad \text{(Eq 12)}$$

where E is the experimental finding and P is the predicted value obtained from the constitutive equation. The $\bar{E}$ and $\bar{P}$ are the mean values of E and P, respectively. The N is the number of data, which are employed in the investigation. The
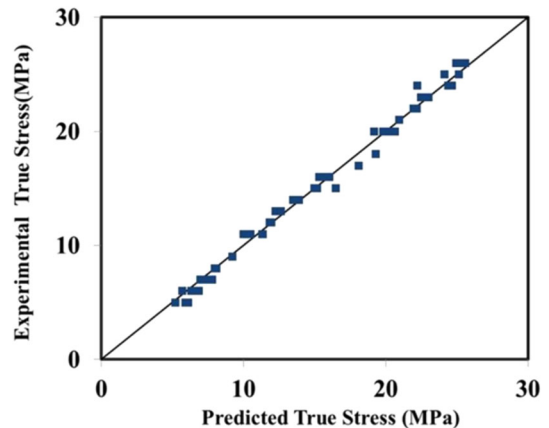
Fig. 10 The correlation between the experimental and predicted flow stress in a temperature range of 1050-1150 °C and a strain rate of 0.0025-0.25 s^{-1} through hot compression of Ti-6Al-7Nb biomedical alloy

correlation coefficient (R), a commonly used statistical parameter, provides information on the strength of linear relationship between the observed and the predicted values, whereas the average absolute relative error (AARE), an unbiased statistical parameter for measuring the predictability of a model/equation, is calculated through a term-by-term comparison of the relative error (Ref 39, 40). As it can be seen in Fig. 10, a good correlation ($R = 0.986$) between experimental and predicted data is obtained. And the average absolute rela-

tive error (AARE) was found to be 4.65%, which indicates the excellent predictability of the developed constitutive equation. All these demonstrate that the developed constitutive equation is appropriate and reliable for the analysis of the hot deformation process of the experimental material.

4. Conclusion

The hot compression tests were conducted on Ti-6Al-7Nb alloy in a temperature range of 1050-1150 °C and strain rates of 0.0025-0.25 s^{-1}. On the basis of experimental data, the dynamic recovery and partial recrystallization were found to be operative during deformation which leads to a broad peak in flow curves. The activation energies for deformation are calculated to be in the range of 161-242 kJ/mol. The critical peak stress for DRX increased by raising strain rates or decreasing deformation temperature. The constitutive equations for the experimental alloy are developed using hyperbolic-sine type equation in the single-phase β region incorporating strain effect. The flow stress model was developed through estimating material constants to describe the deformation temperature and strain rate dependence. The predicted flow stresses were in good agreement with experimental data.

References

1. D. Iijima, T. Yoneyama, H. Doi, H. Hamanaka, and N. Kurosaki, Wear Properties of Ti and Ti–6Al–7Nb Castings for Dental Prostheses, *Biomaterials*, 2003, **24**, p 1519–1524
2. K. Narita, M. Niinomi, M. Nakai, J. Hieda, and K. Oribe, Development of Thermo-mechanical Processing for Fabricating Highly Durable β-type Ti-Nb-Ta-Zr Rod for Use in Spinal Fixation Devices, *J. Mech. Behav. Biomed. Mater.*, 2012, **9**, p 207–216
3. M. Geetha, A.K. Singh, R. Asokamani, and A.K. Gogia, Ti Based Biomaterials, the Ultimate Choice for Orthopaedic Implants—A Review, *Prog. Mater Sci.*, 2009, **54**, p 397–425
4. G. He and M. Hagiwara, Ti Alloy Design Strategy for Biomedical Applications, *Mater. Sci. Eng. C*, 2006, **26**, p 14–19
5. M.F. Semlitsch, H. Weber, R.M. Streicher, and R. Schön, Joint Replacement Components Made of Hot-Forged and Surface-Treated Ti–6Al–7Nb Alloy, *Biomaterials*, 1992, **13**(11), p 781–788
6. D. Samantaray, S. Mandal, A.K. Bhaduri, S. Venugopal, and P.V. Sivaprasad, Analysis and Mathematical Modelling of Elevated Temperature Flow Behaviour of Austenitic Stainless Steels, *Mater. Sci. Eng. A*, 2011, **528**, p 1937–1943
7. N. Bontcheva, G. Petzov, and L. Parashkevova, Thermomechanical Modelling of Hot Extrusion of Al-alloys, Followed by Cooling on the Press, *Comput. Mater. Sci.*, 2006, **38**, p 83–89
8. Y.C. Lin and X.M. Chen, A Critical Review of Experimental Results and Constitutive Descriptions for Metals and Alloys in Hot Working, *Mater. Des.*, 2011, **32**, p 1733–1759
9. Y.C. Lin and G. Liu, A New Mathematical Model for Predicting Flow Stress of Typical High-Strength Alloy Steel at Elevated High Temperature, *Comput. Mater. Sci.*, 2010, **48**, p 54–58
10. N. Haghdadi, A. Zarei-Hanzaki, A.R. Khalesian, and H.R. Abedi, Artificial Neural Network Modeling to Predict the Hot Deformation Behavior of an A356 Aluminum Alloy, *Mater. Des.*, 2013, **49**, p 386–391
11. C.M. Sellars and W.J. McTegart, On the Mechanism of Hot Deformation, *Acta Metall.*, 1966, **14**, p 1136–1138
12. A. Marandi, A. Zarei-Hanzaki, N. Haghdadi, and M. Eskandari, The prediction of Hot Deformation Behavior in Fe–21Mn–2.5 Si–1.5 Al Transformation-Twinning Induced Plasticity Steel, *Mater. Sci. Eng. A*, 2012, **554**, p 72–78
13. H.Y. Li, Y.H. Li, D.D. Wei, J.J. Liu, and X.F. Wang, Constitutive Equation to Predict Elevated Temperature Flow Stress of V150 Grade Oil Casing Steel, *Mater. Sci. Eng. A*, 2011, **530**, p 367–372
14. H.Y. Li, D.D. Wei, J.D. Hu, Y.H. Li, and S.L. Chen, Constitutive Modeling for Hot Deformation Behavior of T24 Ferritic Steel, *Comput. Mater. Sci.*, 2012, **53**, p 425–430
15. M.A. Shafaat, H. Omidvar, and B. Fallah, Prediction of Hot Compression Flow Curves of Ti–6Al–4V Alloy in α + β Phase Region, *Mater. Des.*, 2011, **32**, p 4689–4695
16. J. Cai, F. Li, T. Liu, B. Chen, and M. He, Constitutive Equations for Elevated Temperature Flow Stress of Ti–6Al–4V Alloy Considering the Effect of Strain, *Mater. Des.*, 2011, **32**, p 1144–1151
17. R. Ding, Z.X. Guo, and A. Wilson, Microstructural Evolution of a Ti – 6Al – 4V Alloy During Thermomechanical Processing, *Mater. Sci. Eng. A*, 2002, **327**, p 233–245
18. W. Yu, J. Li, and J. Luo, Effect of Processing Parameters on Microstructure and Mechanical Properties in High Temperature Deformation of Ti-6Al-4V Alloy, *Rare. Metal. Mater. Eng.*, 2009, **38**(1), p 19–24
19. S. Roy and S. Suwas, The Influence of Temperature and Strain Rate on the Deformation Response and Microstructural Evolution During Hot Compression of a Titanium Alloy Ti–6Al–4V–0.1B, *J. Alloy Compd.*, 2013, **548**, p 110–125
20. W.F. Cui, Z. Jin, A.H. Guo, and L. Zhou, High Temperature Deformation Behavior of α + β Type Biomedical Titanium Alloy Ti–6Al–7Nb, *Mater. Sci. Eng. A*, 2009, **499**, p 252–256
21. T. Akahori, M. Niinomi, K.I. Fukunaga, and I. Inagaki, Effects of Microstructure on the Short Fatigue Crack Initiation and Propagation Characteristics of Biomedical α/β Titanium Alloys, *Metall. Mater. Trans. A*, 2000, **31**, p 1949–1958
22. E. Poliak and J. Jonas, A One-Parameter Approach to Determining the Critical Conditions for the Initiation of Dynamic Recrystallization, *Acta Mater.*, 1996, **44**, p 127–136
23. H.J. McQueen, The Discovery of the Dynamic Restoration Mechanisms in Hot Working, *Met. Forum (Australia)*, 1981, **4**, p 81–91
24. H. Mirzadeh, J.M. Cabrera, and A. Najafizadeh, Modeling and Prediction of Hot Deformation Flow Curves, *Metall. Mater. Trans. A*, 2012, **43A**, p 108–123
25. I. Weiss and S.L. Semiatin, Thermomechanical Processing of Beta Titanium Alloys—An Overview, *Mater. Sci. Eng. A*, 1998, **243**, p 46–65
26. W. Jia, W. Zeng, J. Liu, Y. Zhou, and Q. Wang, On the Influence of Processing Parameters on Microstructural Evolution of a Near Alpha Titanium Alloy, *Mater. Sci. Eng. A*, 2011, **530**, p 135–143
27. I. Weiss and F.H. Froes, *Titanium '84: Science and Technology*, G. Lütjering, U. Zwicker, and W. Bunk, Ed., Deutsche Gesellschaft fur Metallkunde E.V, Oberursel, 1985, p 499–506
28. F. Warchomicka, C. Poletti, and M. Stockinger, Study of the Hot Deformation Behaviour in Ti–5Al–5Mo–5V–3Cr–1Zr, *Mater. Sci. Eng. A*, 2011, **528**, p 8277–8285
29. A. Najafizadeh and J.J. Jonas, Predicting the Critical Stress for Initiation of Dynamic Recrystallization, *ISI. J. Int.*, 2006, **46**, p 1679–1684
30. G. Quan, D. Wu, G. Luo, Y. Xia, J. Zhou, Q. Liu, and L. Gao, Dynamic Recrystallization Kinetics in α Phase of as-Cast Ti–6Al–2Zr–1Mo–1 V Alloy During Compression at Different Temperatures and Strain Rates, *Mater. Sci. Eng. A*, 2014, **589**, p 23–33
31. Y. Han, W. Zeng, Y. Qi, and Y. Zhao, Optimization of Forging Process Parameters of Ti600 Alloy by Using Processing Map, *Mater. Sci. Eng. A*, 2011, **529**, p 393–400
32. W. Jia, W. Zeng, Y. Zhou, J. Liu, and Q. Wang, High-Temperature Deformation Behavior of Ti60 Titanium Alloy, *Mater. Sci. Eng. A*, 2011, **528**, p 4068–4074
33. X.G. Fan, H. Yang, and P.F. Gao, Deformation Behavior and Microstructure Evolution in Multistage Hot Working of TA15 Titanium Alloy: on the Role Of Recrystallization, *J. Mater. Sci.*, 2011, **46**, p 6018–6028
34. J. Zhang, H. Di, H. Wang, K. Mao, T. Ma, and Y. Cao, Hot Deformation Behavior of Ti-15-3 Titanium Alloy: A Study Using Processing Maps, Activation Energy Map, and Zener-Hollomon Parameter Map, *J. Mater. Sci.*, 2012, **47**, p 4000–4011
35. J. Luo, M. Li, H. Li, and W. Yu, Effect of the Strain on the Deformation Behavior of Isothermally Compressed Ti–6Al–4V Alloy, *Mater. Sci. Eng. A*, 2009, **505**, p 88–95
36. S.M. Abbasi, M. Morakkabati, A.H. Sheikhali, and A. Momeni, Hot Deformation Behavior of Beta Titanium Ti-13V-11Cr-3Al Alloy, *Metall. Mater. Trans. A*, 2014, **45A**, p 5201–5211

37. R.A. Mulford and U.F. Kocks, New Observations on the Mechanisms of Dynamic Strain Aging and of Jerky Flow, *Acta Metall.*, 1979, **27**, p 1125–1134

38. F. Pilehva, A. Zarei-Hanzaki, M. Ghambari, and H.R. Abedi, Flow Behavior Modeling of a Ti–6Al–7Nb Biomedical Alloy During Manufacturing at Elevated Temperatures, *Mater. Des.*, 2013, **51**, p 457–465

39. N. Haghdadi, A. Zarei-Hanzaki, and H.R. Abedi, The Flow Behavior Modeling of Cast A356 Aluminum Alloy at Elevated Temperatures Considering the Effect of Strain, *Mater. Sci. Eng. A*, 2012, **535**, p 252–257

40. D. Samantaray, S. Mandal, and A.K. Bhaduri, Constitutive Analysis to Predict High-Temperature Flow Stress in Modified 9Cr–1Mo (P91) Steel, *Mater. Des.*, 2010, **31**, p 981–984